Ultrastrong coupling between a microwave resonator and antiferromagnetic resonances of rare-earth ion spins

Jonathan R. Everts,[1] Gavin G. G. King,[1] Nicholas J. Lambert,[1] Sacha Kocsis,[2] Sven Rogge,[2] and Jevon J. Longdell[1]

[1]*The Dodd-Walls Centre for Photonic and Quantum Technologies, Department of Physics, University of Otago, Dunedin 9054, New Zealand*

[2]*Centre for Quantum Computation and Communication Technology, The University of New South Wales, Sydney, New South Wales 2052, Australia*

(Received 11 February 2020; revised manuscript received 17 May 2020; accepted 21 May 2020; published 8 June 2020; corrected 22 June 2020)

Quantum magnonics is a new and active research field, leveraging the strong collective coupling between microwaves and magnetically ordered spin systems. To date work in quantum magnonics has focused on transition metals and almost entirely on ferromagnetic resonances in yttrium iron garnet. Antiferromagnetic systems have gained interest as they produce no stray field, and are therefore robust to magnetic perturbations with narrow, shape independent resonant linewidths. Rare-earth ion spins are also of particular interest as they can exhibit narrow optical and microwave transitions and have large magnetic dipole moments. Here we show experimental evidence of ultrastrong-coupling between a microwave cavity and collective antiferromagnetic resonances (magnons) in a fully concentrated rare-earth crystal. Using a loop-gap microwave resonator a coupling strength of 1.75 GHz is obtained between the cavity and the antiferromagnetic resonances in a $GdVO_4$ sample. Furthermore we measure the linewidth of the antiferromagnetic magnon to be 35 MHz, proving that narrow magnon linewidths can be achieved in rare-earth crystals. The combination of the unique optical and spin properties of the rare earths and collective antiferromagnetic order paves the way for quantum magnonic applications.

DOI: 10.1103/PhysRevB.101.214414

I. INTRODUCTION

Superconducting qubits have provided a set of capabilities in quantum computing, control and measurement. In turn, this has generated much interest in "hybrid quantum systems" [1,2]. In such approaches the superconducting qubits capabilities are enhanced by coupling them to another type of system. Among the challenges that the hybrid approach tries to address is the long term storage of quantum information by using spins, as well as long distance, room temperature, and quantum communication by microwave to optical conversion [3].

Rare-earth ions offer exciting possibilities for quantum information because of the long coherence times available for both their optical [4,5] and optically addressed spin transitions [6]. Quantum memories based on ensembles of rare-earth ions have demonstrated large bandwidths [7], high efficiencies and very long storage times [6].

Rare-earth ions doped in solids are also being investigated for quantum information application [8], including microwave to optical conversion [9–13]. When using rare-earth-doped samples for these applications, there is a tradeoff when it comes to the concentration of the dopant. Higher dopant concentrations cause a desirable increase in the collective coupling strength to electromagnetic waves but an undesirable increase in both homogeneous and inhomogeneous linewidths. For optical transitions in low concentration rare-earth dopants, this increase is often due to Stark shifts or an increase in crystal strain from dopants degrading the crystal quality [14]. For electron spin transitions it is often due to magnetic dipole-dipole interactions [15].

A way out of this concentration-linewidth trade off is to instead use fully concentrated rare-earth crystals where the rare earth is part of the host crystal. In the case of optical transitions it has been shown that very narrow inhomogeneous linewidths (25 MHz)[16] can be achieved in fully concentrated samples, linewidths comparable with the narrowest seen in doped samples [8,17]. Prior to the work presented here, narrow microwave transitions had not been seen in fully concentrated rare-earth crystals, however, in similar high concentration spin materials such as yttrium iron garnet, linewidths on the order of a MHz have been measured [18–20].

Here we investigate the coupling between antiferromagnetic magnon modes in the fully concentrated rare- earth crystal gadolinium vanadate ($GdVO_4$) and a microwave cavity. We show that not only can ultrastrong-coupling be achieved but that the linewidth of the magnon resonances are narrow, an important property for their use in hybrid quantum systems.

The magnetic and thermal properties of fully concentrated rare-earth phosphates and vanadates have been investigated before [21,22], and collective resonances were observed in dysprosium ferrite ($DyFeO_3$) [23], gadolinium aluminate ($GdAlO_4$), and $GdVO_4$. These were observed however, at much higher temperatures and showed much larger linewidths than we observe here. In general antiferromagnetic resonance in rare earth systems is a largely unexplored area.

$GdVO_4$ has a tetragonal crystal lattice with space group $D_{4h}^{19}(I4/amd)$. There are four Gd^{3+} ions per unit cell with site symmetry D_{2d}. At room temperature $GdVO_4$ is paramagnetic but upon cooling at zero-magnetic field to $T \leqslant 2.495$ K, it orders antiferromagnetically as a simple two sublattice system parallel to the crystallographic c axis [24]. The low ordering temperature is a characteristic of rare-earth spins as the exchange interaction between the highly shielded $4f$ electrons is weak, and often the magnetic dipole-dipole interaction dominates [25]. The Gd^{3+} ions are in an $^8S_{7/2}$ ground state, a predominantly $L = 0$ state; crystal field effects are therefore small and the g factor is approximately isotropic with a value of 2. $GdVO_4$ is isostructural with the ubiquitous laser host material yttrium vanadate and is a good laser host in its own right. The sample we used was commerically grown and available off the shelf.

The antiferromagnetic resonance [26,27] seen in our system can be understood by modeling each sublattice by a single spin-1/2 and using the following interaction Hamiltonian:

$$H = AS_1^z S_2^z - \mu_B g \boldsymbol{B} \cdot (\boldsymbol{S}_1 + \boldsymbol{S}_2). \tag{1}$$

The first term describes the (predominantly) magnetic dipole-dipole interaction that causes antiferromagnetic ordering and the second term describes the interaction of the spins with an applied magnetic field.

We take S_1^z to be our upward pointing spin ($S_z^1 \approx \frac{1}{2}$, $S_z^2 \approx -\frac{1}{2}$), and apply a DC magnetic field of strength B_0 along the z axis. Assuming only small excitations of the spins we make the Holstein-Primakoff transformations [28]

$$S_1^z = \tfrac{1}{2} - \hat{a}^\dagger \hat{a}, \tag{2}$$

$$S_2^z = -\tfrac{1}{2} + \hat{b}^\dagger \hat{b}, \tag{3}$$

$$S_1^+ \approx \hat{a}, \tag{4}$$

$$S_2^- \approx \hat{b}, \tag{5}$$

where $\hat{a}$ and $\hat{b}$ are bosonic annihilation operators for a spin excitation (spin flip) on sublattice 1 and 2, respectively. Substituting into Eq. (1) and keeping terms up to second-order in creation/annihilation operators leads to the Hamiltonian

$$H = \hat{a}^\dagger \hat{a}(\omega_0 + g\mu_B B_0) + \hat{b}^\dagger \hat{b}(\omega_0 - g\mu_B B_0), \tag{6}$$

where $\omega_0 = A/2$. Thus in our simple model there are two antiferromagnetic resonance modes each involving Larmor precession of just one sublattice. At zero magnetic field, the two modes are degenerate at a frequency ω_0 that is directly related to the strength of the ordering interaction. The frequency of mode $\hat{a}$, which sees the applied magnetic field in addition to the internal field, increases linearly with applied magnetic field, where as the frequency of mode $\hat{b}$, which sees the applied field opposing the internal field, decreases linearly with applied magnetic field.

Antiferromagnetic resonance in $GdVO_4$ has been seen in electron spin resonance experiments, with a predicted low temperature zero-field frequency of ∼34 GHz [29]. Using a g factor of 2 the antiferromagnetic resonance frequencies predicted by Eq. (6) are plotted in Fig. 1(a). At ∼1.2 T the lower antiferromagnetic resonance branch intercepts the zero-frequency axis. At this point a transition occurs between the antiferromagnetic phase and the spin-flop phase. In the spin-flop phase, the energy penalty associated with having one of the sublattices antialigned with the external field is relieved by the spins switching from the crystal c axis to the crystal a axis, and tilting a small angle θ towards the external field. As the external field is increased, θ increases, eventually returning the crystal to the paramagnetic phase. Beyond the spin-flop transition Eq. (6) no longer holds and spin resonance theory in the spin-flop state is required instead [30]. The magnetic phase in $GdVO_4$ is shown as a function of temperature and magnetic field in Fig. 1(b).

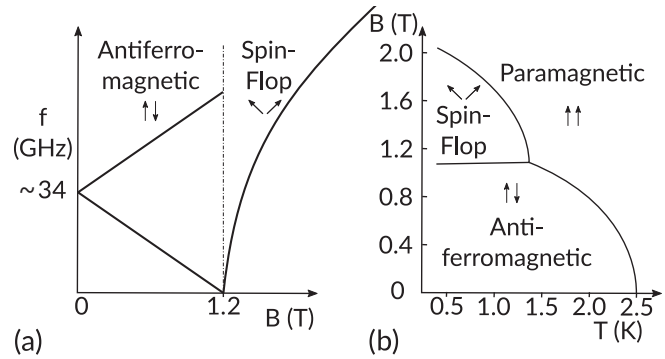

FIG. 1. (a) The antiferromagnetic resonance frequencies of $GdVO_4$ as a function of magnetic field. Beyond the spin-flop transition Eq. (6) no longer holds, spin resonance theory in the spin-flop state is required instead [30]. (b) The magnetic phase diagram of $GdVO_4$ as a function of applied magnetic field strength and temperature [31].

II. EXPERIMENTAL SETUP

The experimental setup used to investigate the coupling between antiferromagnetic modes and a microwave cavity is shown in Fig. 2. A loop-gap microwave resonator [32], with a central frequency of 11.245 GHz and a Q factor of 1300, is mounted on the coldest stage of a dilution fridge (BlueFors LD-250) and inside the bore of a 3 -T superconducting magnet. A 2(a) × 2.5(b) × 2(c) mm $GdVO_4$ sample is mounted in the central hole of the loop-gap resonator where the resonance mode profile is focused and uniform; as shown in Fig. 3. The external DC magnetic field is then applied perpendicular to the AC field and along the crystal c axis, which was identified by observing the crystal through crossed polarizers. Microwaves are coupled into the resonator using two wire antennas attached to SMA (SubMiniature version A) connectors. A vector network analyzer (VNA) is used as the microwave signal source and detector. To reduce the electronic noise the input signal is attenuated at various temperature stages of the dilution fridge, while on the output line a cryoamplifier is used to improve the signal-to-noise ratio. An attenuator is also added between the amplifier and the cavity; this is to suppress heating due to backaction from the input of the amplifier.

The expected coupling strength between the microwave cavity and the antiferromagnetic resonances in our $GdVO_4$

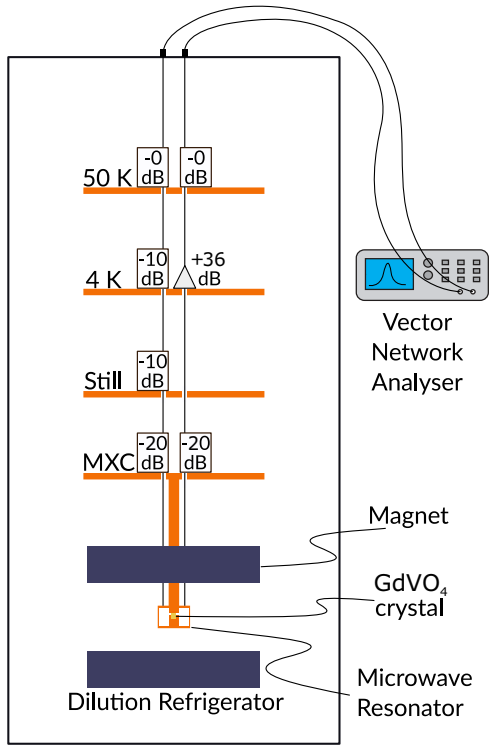

FIG. 2. Schematic of the experimental setup. A $GdVO_4$ sample is placed within a loop-gap microwave resonator that is mounted onto the mixing chamber of a dilution refrigerator. A 3-T superconducting magnet is used to control the magnetic field along the samples crystal c axis and a VNA provides the source and detection of microwave signals through the resonator. The input signal is attentuated at various stages within the refrigerator in order to reduce the electronic thermal noise entering the resonator. A cryoamplifier is then used on the output signal in order to improve the signal to noise ratio at the detector.

sample can be calculated using the following expression [13]:

$$G_\mu = \sqrt{\frac{N\omega_\mu\mu_0}{2\hbar V_\mu}}\mu_B F, \tag{7}$$

where N is the number of Gd^{3+} ions in our sample, ω_μ and V_μ are the central frequency and mode volume of the microwave cavity, respectively, and F is the filling factor.

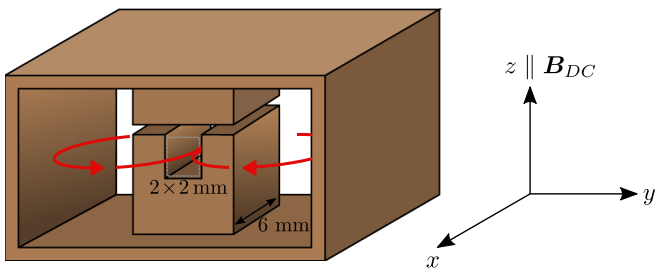

FIG. 3. Schematic of the loop-gap microwave resonator used in our experiment. The resonator is made from oxygen free copper. The square loops form a solenoidal current creating the magnetic field mode indicated by the light red arrows. The $GdVO_4$ sample is placed in the central 2×2mm square hole where $|\boldsymbol{B}_{AC}|$ is maximum.

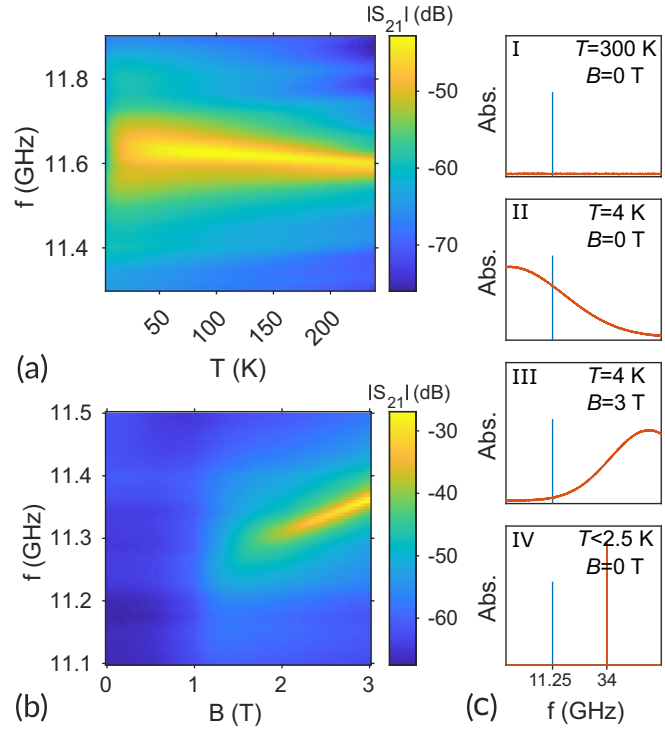

FIG. 4. (a) The cavity transmission as cooled from room temperature to 4 K. (b) Cavity transmission as a function of applied magnetic field with a fixed temperature of $T = 4$ K. (c) A sketch showing the relative locations of the cavity (blue) and spin (orange) resonances at different fields and temperatures.

Approximating the cavity mode volume by the central square gap where the mode is focused and the filling factor by $F = 0.8$ we calculate $G \approx 1.72$ GHz.

III. EXPERIMENTAL RESULTS

Figure 4(a) shows the transmission through the cavity as the cavity is cooled from room temperature to 4 K, with zero applied magnetic field. With decreasing temperature the resonance frequency of the cavity is seen to increase and broaden until the resonance completely disappears at $T \leqslant 35$ K. This occurs due to the interaction between the cavity and the spins. At 300 K, there is a *very* broad paramagnetic resonance centered on 0 Hz. Because it is so broad there is very little absorbtion at the cavity frequency. As the temperature decreases, spin lattice relaxation decreases and the spins resonance narrows, leading to more loss at the cavity frequency. Once the temperature reaches 4 K the attenuation has increased to the point that the cavity resonance disappears. The relative location of the cavity and paramagnetic resonance as the cavity is cooled to 4 K is sketched in Fig. 4(c) I and II.

Keeping the temperature fixed at 4 K an external field is applied (along the crystals c axis) to shift the paramagnetic resonance of the ions away from the cavity, as depicted in Fig. 4(c) III. In Fig. 4(b) we see that as the magnetic field increases and the resonance of the ions is moved, the source of loss to the cavity is reduced allowing the cavity resonance to reappear.

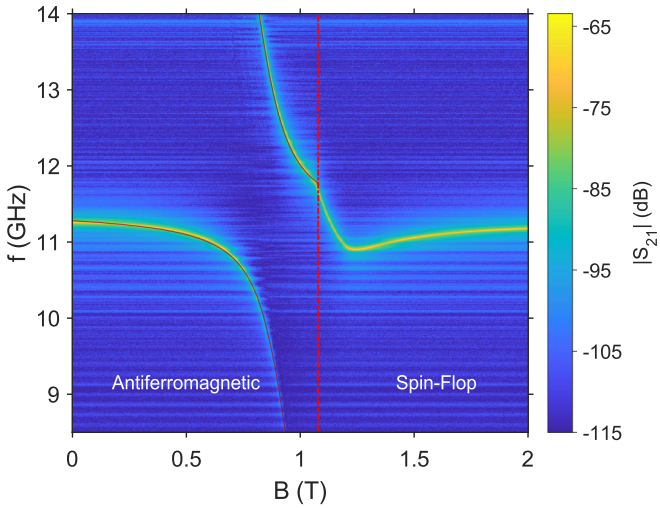

FIG. 5. $T = 25$ mK, transmission through the cavity as a function of magnetic field and frequency. The vertical dashed red line indicates the onset of the spin-flop phase. The fitted eigenvalues of Eq. (8) have been plotted above the transmission data in the antiferromagnet phase.

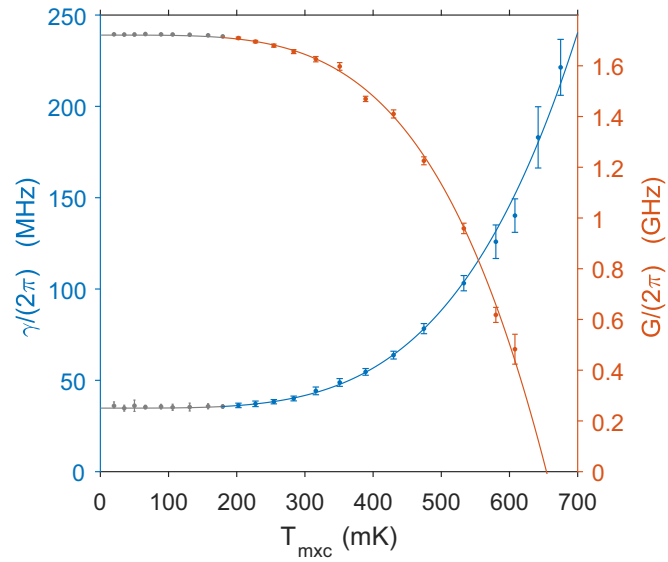

FIG. 6. Blue line is the polariton linewidth measured at a fixed frequency of 15.6 GHz as a function of the mixing chamber temperature, Orange line is the coupling strength G obtained from fitting the eigenvalues of the coupling Hamiltonian Eq. (8). The grey points indicate the region where we have not ruled out the possibility that the mixing chamber and the sample are different temperatures.

The cavity resonance also reappears when the sample is cooled past the transition temperature $T \leqslant 2.495$ K. Below the transition temperature the spins become locked together in a long-range order giving a narrow resonant peak at the zero field antiferromagnetic resonance frequency, ∼34 GHz. As depicted in Fig. 4(c) IV, the cavity is well detuned from this peak and hence resonates as if it were empty.

To investigate the coupling between the antiferromagnetic resonant mode and the microwave cavity, the cavity transmission is measured as the lower antiferromagnetic resonant branch (shown in Fig. 1) is pulled through the cavity resonance via sweeping the applied magnetic field. With the temperature fixed at 25 mK Fig. 5(a) shows the cavity transmission as a function of applied magnetic field. As the lower antiferromagnetic resonant branch passes through the cavity resonance a clear avoided crossing is seen centered at ≈0.9 T. The shape is not symmetric, there is a significant bump in the dressed state frequency at ≈1.1 T due to the onset of the spin-flop transition. A detailed investigation of this phenomenon will be left to future work.

We fit to our data (for $B < 1.1$ T) the eigenvalues of the following coupling Hamiltonian:

$$H = \omega_c \hat{c}^\dagger \hat{c} + \omega_m \hat{m}^\dagger \hat{m} + G(\hat{c}^\dagger + \hat{c})(\hat{m}^\dagger + \hat{m}), \qquad (8)$$

where $\omega_c(\omega_m)$ is the resonant frequency of the cavity mode $\hat{c}$ (magnon mode $\hat{m}$) and $G = \sqrt{N}g$ is the coupling strength, proportional to the number of spins N and single ion coupling strength g. From the fit we obtain a coupling strength of $G/(2\pi) = 1.75$ GHz, which divided by the central frequency of the cavity ($\omega_0/(2\pi) = 11.245$ GHz) gives a coupling figure of $G/\omega_0 = 0.15$ putting the system in the ultrastrong coupling regime [33].

Measuring the linewidth of the polariton modes at points far away from the central cavity frequency gives us an estimate for the linewidth of the antiferromagnetic resonant mode. In order to avoid the background frequency dependence of the experimental components (cables/attenuators/amplifier) we measure the magnetic linewidth of the polariton, that is for a fixed microwave frequency we measure the full width at half maximum of the power transmission as a function of magnetic field. This linewidth (ΔB) measured in Tesla is then converted into a frequency domain linewidth (γ) via the relation $\hbar\gamma = g\mu_B\Delta B$.

Fixing the frequency at 15.6 GHz the linewidth of the upper polariton branch was measured as a function of the mixing chamber temperature (T_{mxc}), as shown in Fig. 6. As the temperature of the mixing chamber is lowered the magnon linewidth reduces until a temperature of $T_{\text{mxc}} \leqslant 200$ mK where the linewidth remains roughly constant at $\gamma/(2\pi) \sim 35$ MHz. The reduction in linewidth with temperature is expected because of a reduction in multimagnon processes [34,35]. In the low temperature limit four-magnon processes are shown to dominate and a T^4 linewidth dependence is predicted. The constant linewidth we see for $T_{\text{mxc}} \leqslant 200$ mK could be due to some nonmagnetic broadening mechanism, however it could also be explained by a temperature mismatch between the mixing chamber and the sample. The spins in our sample are not only coupled to phonons in the host lattice but also to microwave photons in the cavity and therefore the system equilibrates at an intermediate temperature that depends on the strength of the coupling to each reservoir [36]. At millikelvin temperatures the thermal conductivity of the $GdVO_4$ sample will become very small, making cooling the spins via thermal contact with the mixing chamber difficult. The smooth line shown behind the linewidth data points is a fit to the equation $\gamma = A + BT^4$, where the coefficients were calculated as $A/(2\pi) = 34.8$ MHz and $B/(2\pi) = 860$ MHz/K^4. The low temperature required to achieve narrow linewidths could be

seen as an issue from an application stand point, however, superconducting qubit platforms in which our system could find application, are already required to operate at dilution refrigerator temperatures.

The coupling strength G measured via fitting the eigenvalues of Eq. (8) is also shown as a function of T_{mxc} in Fig. 6. The coupling strength follows a similar trend to the linewidth data, remaining constant at $G/(2\pi) \sim 1.75$ GHz up until $T_{\mathrm{mxc}} \approx 200$ mK after which it starts decreasing proportional to T^4. Fitting the expression $G = C - DT^4$ gives coefficients $C/(2\pi) = 1.7$ GHz and $D/(2\pi) = 9.39$ GHz/K^4.

IV. CONCLUSION AND OUTLOOK

Our results put us in the ultrastrong coupling regime, $G/\omega_0 = 0.15 > 0.1$, the region where counter rotating terms in the coupling Hamiltonian start to become significant. With a lower frequency resonator ($\leqslant 1.7$ GHz) the deep strong coupling regime could be reached. The challenge will be keeping narrow magnon linewidths in spite of this low frequency, which will require low spin temperatures to maintain high spin order. The construction of a tunable microwave resonator to explore cavity coupling at different frequency positions along the antiferromagnetic resonant branches is a task we are working on for future experiments.

The narrow collective magnetic resonance measured here in combination with the narrow optical linewidths rare-earth crystals are already well known for having significant implications for microwave to optical conversion application. $GdVO_4$, however, is unlikely to be the best material for this. The Gd^{3+} ions have half filled $4f$ orbitals and as a result the lowest energy $4f - 4f$ transition from the ground state is in the ultraviolet spectrum around 315 nm. Unfortunately the VO_4^{3-} ions absorb strongly at this wavelength. Different rare-earth crystals with better optical properties for upconversion will be the subject of future work.

Another exciting prospect provided by rare-earth ions is the large spectroscopic g factors available, particularly in erbium and dysprosium where $g \approx 15$ is common. With this the collective coupling, which is linear in g, could be further improved.

Our measurements show that narrow collective magnetic resonances occur in rare-earth crystals. In comparison to rare-earth-doped samples the concentration to linewidth ratio seen here is orders of magnitude higher. Quantum magnonics using rare-earth crystals has an exciting future. The remarkable properties of the rare-earth $4f - 4f$ transitions, the easy accessibility of antiferromagnetic resonances as well as the large g factors, open up many possibilities for improvements to hybrid quantum systems.

ACKNOWLEDGMENTS

The authors thank R. Ahlefeldt, M. Berrington, and M. Sellars for valuable discussions. This work was supported by Army Research Office (ARO/LPS) (CQTS) Grant No. W911NF1810011, the Marsden Fund (Contract No. UOO1520) of the Royal Society of New Zealand, the ARC Centre of Excellence for Quantum Computation and Communication Technology (Grant No. CE170100012), the Discovery Project (Grant No. DP150103699) and the MBIE of New Zealand Endeavour Smart Ideas fund (Contract No.UOOX1805).

[1] D. Lachance-Quirion, Y. Tabuchi, A. Gloppe, K. Usami, and Y. Nakamura, Appl. Phys. Express **12**, 070101 (2019).
[2] G. Kurizki, P. Bertet, Y. Kubo, K. Mølmer, D. Petrosyan, P. Rabl, and J. Schmiedmayer, Proc. Natl. Acad. Sci. **112**, 3866 (2015).
[3] N. J. Lambert, A. Rueda, F. Sedlmeir, and H. G. L. Schwefel, Adv. Quantum Technol. **3**, 1900077 (2020).
[4] R. W. Equall, Y. Sun, R. L. Cone, and R. M. Macfarlane, Phys. Rev. Lett. **72**, 2179 (1994).
[5] T. Böttger, C. W. Thiel, Y. Sun, and R. L. Cone, Phys. Rev. B **74**, 075107 (2006).
[6] M. Zhong, M. P. Hedges, R. L. Ahlefeldt, J. G. Bartholomew, S. E. Beavan, S. M. Wittig, J. J. Longdell, and M. J. Sellars, Nature (London) **517**, 177 (2015).
[7] C. Clausen, I. Usmani, F. Bussières, N. Sangouard, M. Afzelius, H. d. Riedmatten, and N. Gisin, Nature (London) **469**, 508 (2011).
[8] C. W. Thiel, T. Böttger, and R. L. Cone, J. Lumin. **131**, 353 (2011), Selected papers from DPC'10.
[9] C. O'Brien, N. Lauk, S. Blum, G. Morigi, and M. Fleischhauer, Phys. Rev. Lett. **113**, 063603 (2014).
[10] L. A. Williamson, Y.-H. Chen, and J. J. Longdell, Phys. Rev. Lett. **113**, 203601 (2014).
[11] X. Fernandez-Gonzalvo, S. P. Horvath, Y.-H. Chen, and J. J. Longdell, Phys. Rev. A **100**, 033807 (2019).
[12] S. Welinski, P. J. T. Woodburn, N. Lauk, R. L. Cone, C. Simon, P. Goldner, and C. W. Thiel, Phys. Rev. Lett. **122**, 247401 (2019).
[13] J. R. Everts, M. C. Berrington, R. L. Ahlefeldt, and J. J. Longdell, Phys. Rev. A **99**, 063830 (2019).
[14] M. J. Sellars, E. Fraval, and J. J. Longdell, J. Lumin. **107**, 150 (2004), Proceedings of the 8th International Meeting on Hole Burning, Single Molecule, and Related Spectroscopies: Science and Applications.
[15] R. S. d. Biasi and A. A. R. Fernandes, J. Phys. C **16**, 5481 (1983).
[16] R. L. Ahlefeldt, M. R. Hush, and M. J. Sellars, Phys. Rev. Lett. **117**, 250504 (2016).
[17] R. M. Macfarlane, R. S. Meltzer, and B. Z. Malkin, Phys. Rev. B **58**, 5692 (1998).
[18] Y. Tabuchi, S. Ishino, T. Ishikawa, R. Yamazaki, K. Usami, and Y. Nakamura, Phys. Rev. Lett. **113**, 083603 (2014).
[19] M. Goryachev, W. G. Farr, D. L. Creedon, Y. Fan, M. Kostylev, and M. E. Tobar, Phys. Rev. Appl. **2**, 054002 (2014).
[20] S. Klingler, H. Maier-Flaig, C. Dubs, O. Surzhenko, R. Gross, H. Huebl, S. T. B. Goennenwein, and M. Weiler, Appl. Phys. Lett. **110**, 092409 (2017).
[21] B. Bleaney, Appl. Magn. Reson. **19**, 209 (2000).
[22] G. J. Bowden, Aust. J. Phys. **51**, 201 (1998).

[23] M. Białek, A. Magrez, and J.-P. Ansermet, Phys. Rev. B **101**, 024405 (2020).
[24] J. Cashion, A. Cooke, L. Hoel, D. Martin, and M. Wells, in *Élements des terres rares*, Vol. 2, Centre National de la Recherche Scientifique (Paris) (Éditions du Centre National de la Recherche Scientifique, Paris, 1970) pp. 417–426.
[25] E. Lagendijk, H. W. J. Blöte, and W. J. Huiskamp, Physica **61**, 220 (1972).
[26] C. Kittel, Phys. Rev. **82**, 565 (1951).
[27] H. Y. Yuan and X. R. Wang, Appl. Phys. Lett. **110**, 082403 (2017).
[28] T. Holstein and H. Primakoff, Phys. Rev. **58**, 1098 (1940).
[29] M. M. Abraham, J. M. Baker, B. Bleaney, J. Z. Pfeffer, and M. R. Wells, J. Phys.: Condens. Matter **4**, 5443 (1992).
[30] W. Yung-Li and H. B. Callen, J. Phys. Chem. Solids **25**, 1459 (1964).
[31] B. Mangum and D. Thornton, in *Magnetism and Magnetic Materials - 1971 Parts 1 and 2*, edited by C. D. Graham and J. J. Rhyne, AIP Conf. Proc No. 5 (AIP, New York, 1972), p. 311.
[32] J. R. Ball, Y. Yamashiro, H. Sumiya, S. Onoda, T. Ohshima, J. Isoya, D. Konstantinov, and Y. Kubo, Appl. Phys. Lett. **112**, 204102 (2018).
[33] A. F. Kockum, A. Miranowicz, S. D. L. amd Salvatore Savasta, and F. Nori, Nat. Rev. Phys. **1**, 19 (2019).
[34] S. M. Rezende and R. M. White, Phys. Rev. B **14**, 2939 (1976).
[35] S. Rezende and R. White, Physica B+C. **86-88**, 1277 (1977).
[36] B. Albanese, S. Probst, V. Ranjan, C. Zollitsch, M. Pechal, A. Wallraff, J. Morton, D. Vion, D. Esteve, E. Flurin, and P. Bertet, Nat. Phys. (2020), doi: 10.1038/s41567-020-0872-2.

Correction: The surname of the last author contained an error and has been fixed.